Available online at www.sciencedirect.com
ScienceDirect
Journal of Power Sources 161 (2006) 843–848
JOURNAL OF POWER SOURCES
www.elsevier.com/locate/jpowsour

Effects of hydrophilic/hydrophobic properties on the water behavior in the micro-channels of a proton exchange membrane fuel cell

Y.H. Cai [a,b], J. Hu [a], H.P. Ma [a,b], B.L. Yi [a,*], H.M. Zhang [a]

[a] *Fuel cell R&D Center, Dalian Institute of Chemical Physics, Chinese Academy of Sciences, 457 Zhongshan Road, Dalian 116023, PR China*
[b] *Graduate School of Chinese Academy of Sciences, Beijing 100039, PR China*

Received 6 April 2006; received in revised form 27 April 2006; accepted 27 April 2006
Available online 9 June 2006

Abstract

The mobility of water droplets and water films inside a straight micro-channel of a proton exchange membrane fuel cell was simulated to study the effects of the hydrophilic/hydrophobic properties on water behavior. The volume-of-fluid model in the FLUENT package was used to keep track of the deformation of the liquid–gas interface. The results show that the water moved faster on a hydrophobic surface. But a hydrophobic channel side-wall was a disadvantage for the gas diffusion when the MEA had a hydrophilic surface. A hydrophilic channel side-wall with a hydrophobic MEA surface could avoid water accumulation on the MEA surface. The water and gas distribution under this condition was advantageous for water discharge and gas diffusion.

Keywords: Proton exchange membrane fuel cells; Water transport; Hydrophilic; Hydrophobic; Two-phase flow

1. Introduction

Proton exchange membrane fuel cells (PEMFCs) are of great potential use in mobile and stationary applications. However, the performance of contemporary PEMFCs needs to be significantly improved. Water behavior in PEMFCs has been considered as a key influencing factor on the cell performance. Water management in PEMFCs has been the subject of several studies. Most of these studies were focused on water transportation inside the proton exchange membrane [1–4] and in the gas diffusion layer [5,6]. However, water transport along the gas flow channels should also be considered.

In past decades, water transport inside the gas flow channel was usually modeled as a component of an overall fuel cell model. The effects of water on the gas concentration and the cell performance were simulated [7,8]. The other type of model was a hydraulic model. The deformation of a droplet was studied with the solution of the Navier-Stokes equation [9,10]. Also, the fluid dynamics and liquid water distribution in a serpentine micro-channel or a straight channel were studied by this method [11–14]. Experimental methods such as the neutron imaging method [15–17] and a transparent PEMFC [18,19] were introduced to study the water behavior in the flow fields recently. But it is difficult to separate the water in the membrane and in the gas diffusion layer.

It is known that the geometry of the micro-channel and the hydrophilic/hydrophobic properties of the MEA surface could influence water removal. But reports on the effect of the hydrophilic/hydrophobic properties of the channel side-wall on water removal are rare. In this present work, a three-dimensional fluid dynamic numerical simulation is presented and the water behavior in the straight channel under different material properties is studied. The commercial computational fluid dynamics software, the FLUENT package was used.

2. Computational methodology and the boundary conditions

2.1. Computational domain

The straight channel flow field is typical and used in the fuel cell stack broadly. In this study, part of a straight channel is chosen as the computational domain, as shown in Fig. 1. The

* Corresponding author. Tel.: +86 411 84379097; fax: +86 411 84684839.
E-mail address: blyi@dicp.ac.cn (B.L. Yi).

0378-7753/$ – see front matter © 2006 Elsevier B.V. All rights reserved.
doi:10.1016/j.jpowsour.2006.04.110

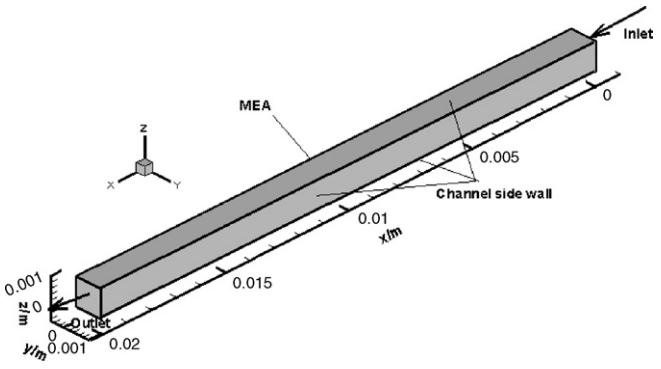

Fig. 1. Computational domain. A part of a straight channel in a PEMFC.

length of the straight channel is 20 mm, and the cross-section is 1 mm × 1 mm.

2.2. Computational methodology

The motion of the gas and the water in the domain could be considered as an incompressible Newtonain flow, one phase flowing past the other phase. The interface that separates the two phases has a constant surface tension σ. When the gas phase is forced to pass a stationary liquid phase, the pressure difference across the liquid phase tends to move the liquid in the direction of the gas flow. Shear forces resulting from the surrounding fluid try to deform the liquid continuous surface. The surface tension forces tend to keep the continuous liquid phase spherical and attached to the wall surface. If the gas flow is strong enough, the distorting forces outweigh the surface tension force and the adhesion force between the liquid phase and the wall. Under this condition, the continuous liquid phase may break up into several fragments.

In this study, the flow in the channel is supposed to be laminar under isothermal conditions and without phase change. A volume-of-fluid (VOF) method in the FLUENT package was adopted to simulate the two-phase flow in a micro-channel. A volume fraction, α_i, is introduced to capture the interface motion. Here, $\alpha = 0$ indicates that the control volume is full with gas, $\alpha = 1$ indicates that the control volume is full with liquid water, and α between zero and unity indicates that the control volume contains the interface between the fluids. The tracking of the interface is accomplished by the solution of a continuity equation for the volume fraction of one phase. The velocity field is continuous across the interface, but there is a pressure jump at the interface due to the presence of surface tension. Therefore, the conservation equations governing an unsteady laminar two-phase flow can be written as [20]:

- Continuity equation:

$$\frac{\partial \rho}{\partial t} + \nabla \cdot (\rho \vec{v}) = 0 \tag{1}$$

- Volume fraction continuity equation:

$$\frac{\partial \alpha_i}{\partial t} + \vec{v} \cdot \nabla(\alpha_i) = 0 \tag{2}$$

- Momentum equation:

$$\frac{\partial}{\partial t}\rho\vec{v} + \nabla \cdot (\rho\vec{v}\vec{v}) = -\nabla p + \nabla \cdot [\mu(\nabla\vec{v} + \nabla\vec{v}^T)] + \rho\vec{g} + \vec{F} \tag{3}$$

In this two-phase system, the gas phase was set as primary phase and represented by the subscript 1, and the liquid phase was set as secondary phase and represented by the subscript 2. So,

$$\alpha_1 + \alpha_2 = 1 \tag{4}$$

The density and the viscosity in each cell can be computed as the following:

$$\rho = \alpha_2\rho_2 + (1 - \alpha_2)\rho_1 \tag{5}$$

$$\mu = \alpha_2\mu_2 + (1 - \alpha_2)\mu_1 \tag{6}$$

In the momentum equation, p is the static pressure, $\rho\vec{g}$ the mass force term, and $\vec{F}$ is the momentum source term due to surface tension and wall adhesion. The continuum surface force model was used. The source term can be written as a function of the surface tension coefficient σ and the surface curvature k, as following form:

$$\vec{F} = 2\sigma k \alpha_2 \nabla \alpha_2 \tag{7}$$

And the calculation of the surface curvature k has a close relationship with the contact angle at the wall.

2.3. Boundary conditions

A no-slip boundary condition is applied to all interior walls. The velocity inlet boundary condition is set at the inlet of the channel. The velocity here is set at 5 m s^{-1}. The gas phase is air. The operating temperature and the pressure is 333 K and 0.2 MPa respectively. Gravity is in the z+ direction.

2.4. Validation of grid independency

A 40,000 hexahedral meshes are employed in the computational domain. The grid independency was validated by various numbers of hexahedral meshes. Whether the meshes number was an additional 50% in the x-direction or 20% in every direction, the simulation results were almost the same. But obviously the computational cost increased. Considering the processing time limitation, 40,000 hexahedral meshes was adopted for all simulation cases.

3. Results and discussion

In this study, six cases were calculated to investigate the water behavior under different hydrophilic/hydrophobic conditions as shown as Table 1. Cases 1 and 2 simulated a single droplet motion on a hydrophilic/hydrophobic surface, respectively. Cases 3 and 4 simulated the influence of the channel material properties on the motion of the water film. Cases 5 and 6 simulated the water film motion on a heterogeneous surface.

Table 1
Simulation cases for different material properties in a micro-channel of PEMFC

Case No.	Initial water distribution	θ_{MEA} [a]	θ_{chan} [b]
1	Single droplet attached to the MEA surface, $V_l = 3.3 \times 10^{-2}$ mm^3	150°	60°
2	Single droplet attached to a side-wall of channel, $V_l = 3.3 \times 10^{-2}$ mm^3	150°	60°
3	A water film with thickness of 0.1 mm covering part of a MEA, $V_l = 1$ mm^3	10°	10°
4	As the same as case 3	10°	150°
5	Two water films with thickness of 0.1 mm covering the hydrophilic part of the MEA, $V_l = 1$ mm^3	θ_{MEA} [c]	10°
6	As the same as case 5	θ_{MEA} [c]	150°

[a] The contact angle at the surface of a MEA.
[b] The contact angle at the wall of the micro-channel.
[c] The surface of the MEA is heterogeneous, and θ_{MEA} is 10° at the hydrophilic part and 150° at the hydrophobic part as shown in Fig. 7.

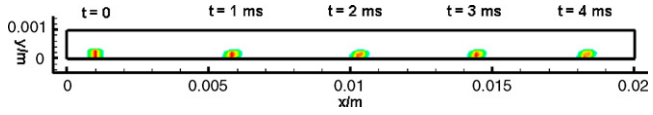

Fig. 2. Single droplet motion at different time instants on a hydrophobic surface.

3.1. Single droplet behavior on a hydrophobic/hydrophilic surface

In case 1, a single droplet was initialized attaching to the surface of MEA near the channel inlet. The volume of the droplet was 3.3×10^{-2} mm^3. The contact angle at the MEA surface was 150°. Fig. 2 shows the single droplet motion at different time instants at the section of $z = 0.0005$ m. The color indicates the liquid phase. At $t = 0$, a single droplet was initialized attached to the surface of the MEA. After $t = 4.6$ ms, the droplet was swept out of the channel. Fig. 3 shows the results calculated from case 2. The liquid water volume was the same as that in case 1. The droplet was initially attached to a hydrophilic surface. The contact angle was 10°. After 5.8 ms the droplet was discharged. Comparing with Fig. 2, shows that the water droplet is removed faster and easier on a hydrophobic surface.

3.2. Liquid water film behavior on a hydrophilic/hydrophobic channel side-wall

In cases 3 and 4, the contact angle at the MEA was 10° and the contact angle of the channel side-wall was 10° and 150°, respectively. In these cases, a liquid water film with thickness of 0.1 mm was initialized covering half of the MEA surface, and the volume of the liquid was 1 mm^3. Fig. 4 shows the liquid water flow rate at the outlet of cases 3 and 4. The results show that it spent less time for a hydrophobic channel to sweep out the water. However, the function of the channel is not only to discharge the water, but also to transport the reactant. Figs. 5 and 6 are the water distributions for cases 3 and 4 at the time $t = 2$ ms. Fig. 5 shows that the water film was gradually spread from the MEA surface to the channel side-wall. Hence a no-water-zone

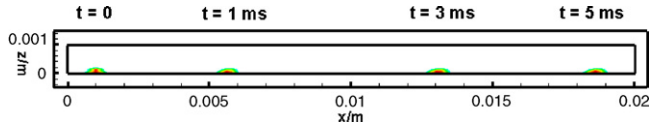

Fig. 3. Single droplet motion at different time instants on a hydrophilic surface.

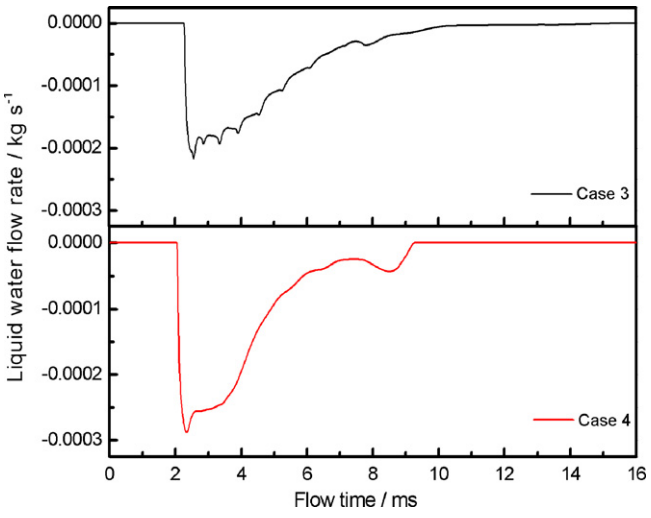

Fig. 4. Liquid water flow rate at the outlet for cases 3 and 4.

on the center of the MEA surface appeared. This phenomenon is beneficial to gas diffusion. Fig. 6 is the water distribution for case 4. It can be seen that water did not spread to the channel side-wall, but covered the MEA surface. This is a disadvantage for gas transport into the MEA.

3.3. The motion of the liquid water film on a heterogeneous surface

The motion of liquid water on a heterogeneous surface was simulated in cases 5 and 6. In these two cases, the surface of

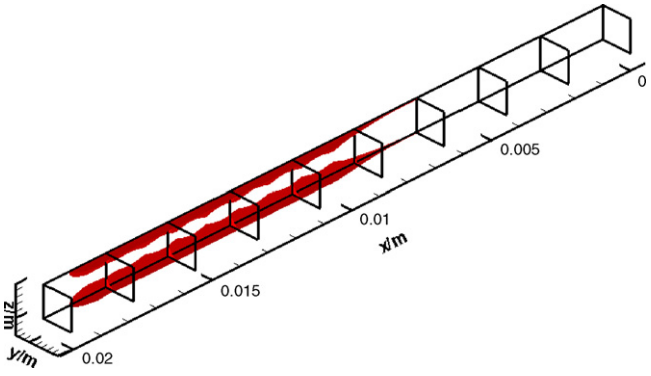

Fig. 5. Water film on the cross sections normal to the flow direction for case 3 at $t = 2$ ms.

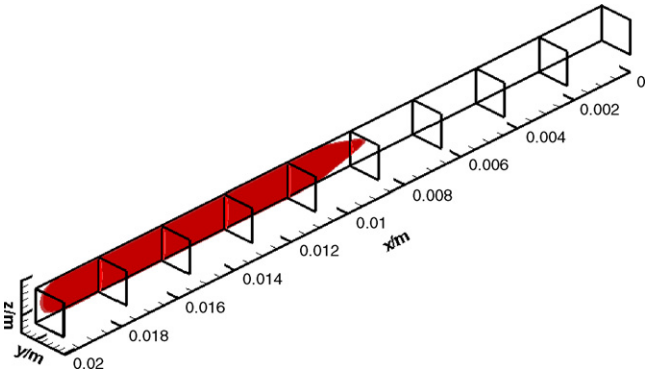

Fig. 6. Water film on the cross sections normal to the flow direction for case 4 at $t = 2$ ms.

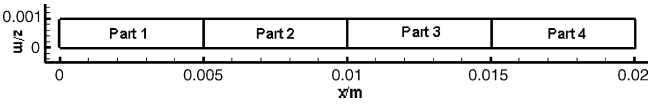

Fig. 7. A sketch of a heterogeneous MEA surface. Parts 1 and 3 were hydrophilic parts and the contact angle was 10°, parts 2 and 4 were hydrophobic parts and the contact angle was 150°.

MEA was divided into four parts averaged as shown in Fig. 7. Parts 1 and 3 were hydrophilic zones and the contact angle of the MEA surface was 10°, then parts 2 and 4 were hydrophobic zones and the contact angel of the MEA surface was 150°. The contact angle of the channel side-wall was 10° in case 5 and 150° in case 6. At the beginning, two water films with the total volume of 1 mm^3 were initialized covering the surface of parts 1 and 3.

Fig. 8 is a comparison of water flow rate at the outlet. The figure shows that water discharging in a hydrophobic channel was faster and more fluent. Fig. 9(a) and (b) are water distribution maps at $t = 3$ and 16 ms for case 5. At first, the water film covering the surface of parts 1 and 3 spreads to the hydrophilic channel side-wall and is moved to parts 2 and 4. Then the water film was split into small water films attached to the channel surface and small droplets were suspended freely in the channel.

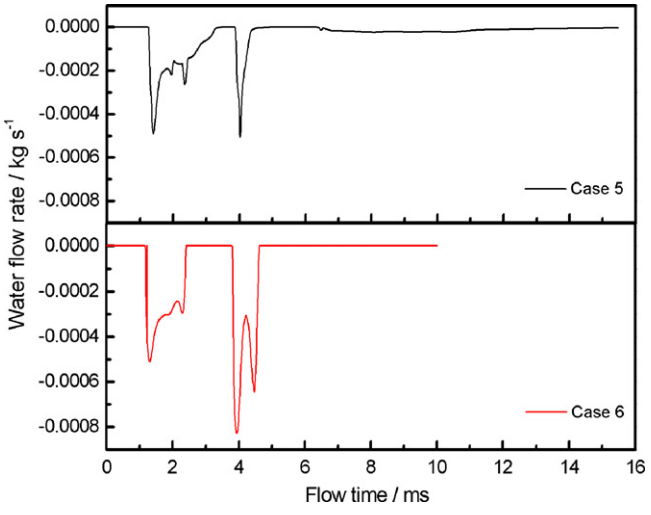

Fig. 8. Liquid water flow rate at the outlet for cases 5 and 6.

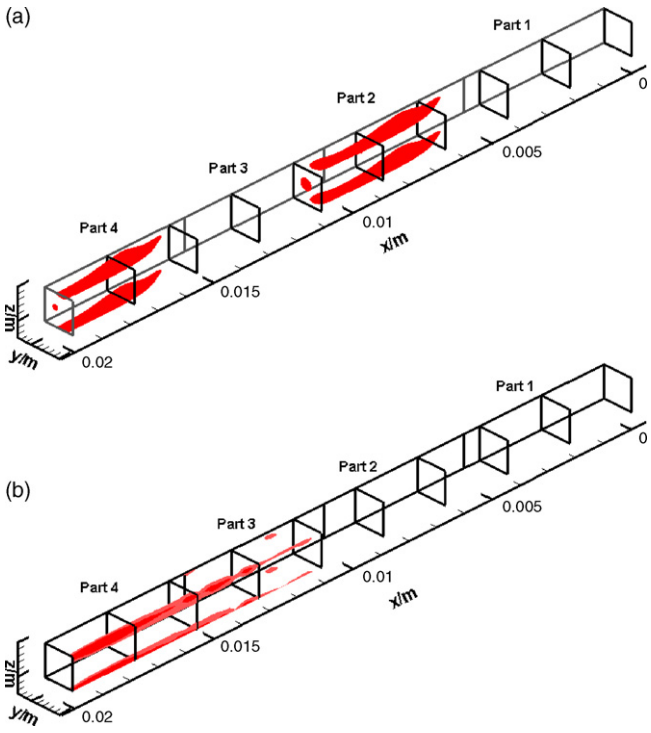

Fig. 9. Water film on the cross sections normal to the flow direction for case 5 at different times: (a) $t = 3$ ms; (b) $t = 16$ ms.

The velocity of the water droplets was faster than that of the water film. So most of water was discharged as water droplets. The water film attached to a hydrophilic surface was difficult to remove. As shown in Fig. 9(b), some of water still existed after 16 ms, accumulating at the corner of the channel.

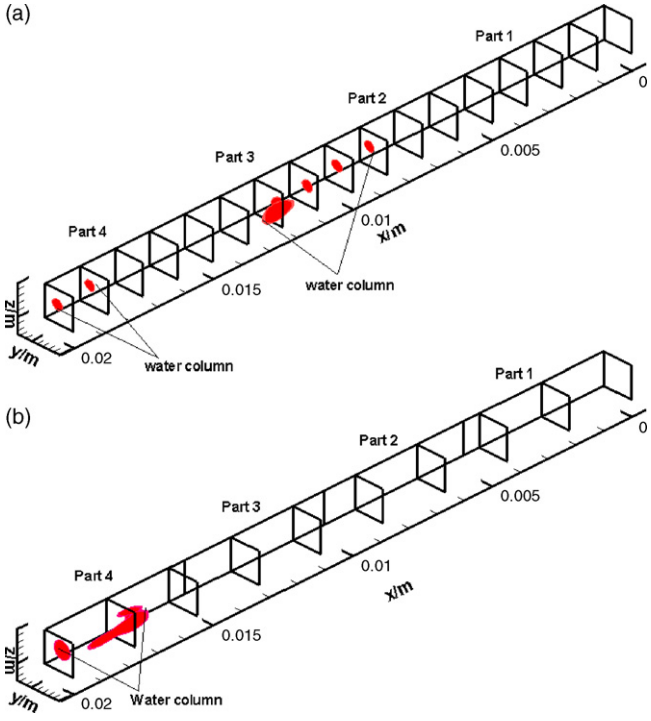

Fig. 10. Water film on the cross sections normal to flow direction for case 6: (a) $t = 2$ ms; (b) $t = 4$ ms.

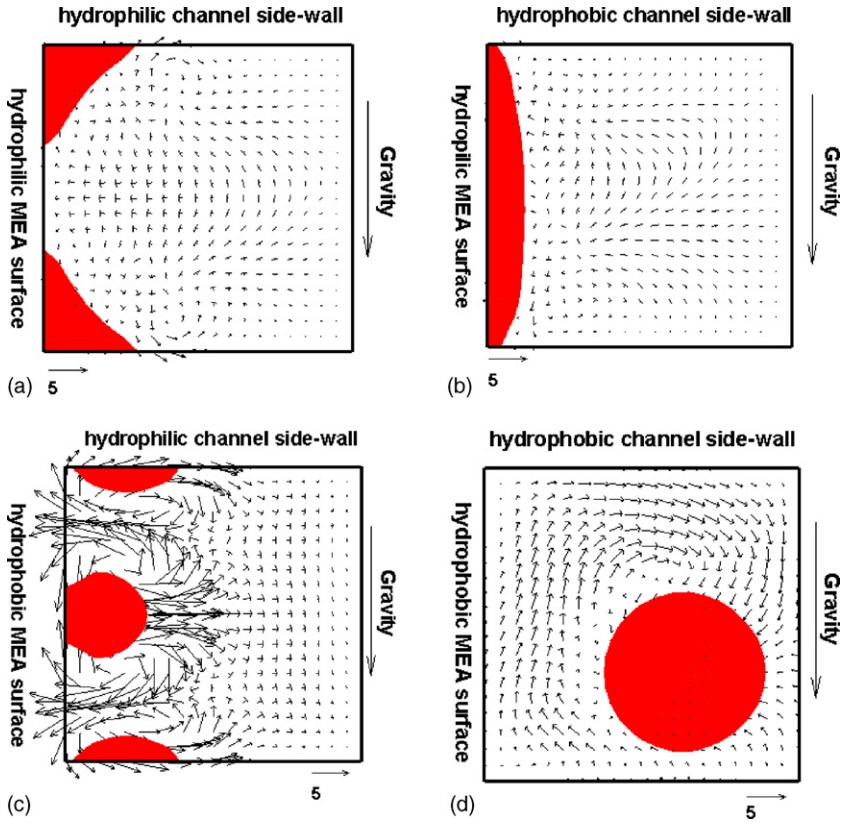

Fig. 11. Water and velocity distribution in a cross-section of a micro-channel with different material properties: (a) hydrophilic MEA surface and hydrophilic channel side-wall; (b) hydrophilic MEA surface and hydrophobic channel side-wall; (c) hydrophobic MEA surface and hydrophilic channel side-wall; (d) hydrophobic MEA surface and hydrophobic channel side-wall.

Fig. 10(a) and (b) are the water distributions at $t = 2$ and 4 ms for case 6. The figures show that water spread onto the hydrophilic MEA surface in parts 1 and 3, but did not spread to a hydrophobic channel side-wall surface. In parts 2 and 4, the water existed as a water column in the micro-channel because the MEA surface was changed to be hydrophobic. The discharge of the water column was faster than that of a water film compared with case 5. But if the water column diameter was large, the channel would be blocked and the gas was hard to transport into the gas diffusion layer.

3.4. Comparison of water and gas distribution under different conditions

In this section, the water distribution and the velocity vectors distribution were compared to research the material properties match of the MEA and the channel side-wall.

In Fig. 11(a), hydrophilic MEA surface was matched with a hydrophilic channel side-wall. Under this condition, part of water spread to the channel, and a part of the MEA surface was exposed to the gas phase. This was beneficial for gas transport into the MEA. But water was adhesive on the surface as a water film and was difficult to be swept out.

Fig. 11(b) shows the worst scenario for fuel cell operation. A thick water film covers the surface of the MEA when a hydrophilic MEA surface was matched with a hydrophobic channel side-wall. In this case the reactant was hard to transport into the MEA.

In Fig. 11(c), the cell had a hydrophobic MEA surface and a hydrophilic channel. Water was separated into water films and water droplets. Water films attached to the hydrophilic channel surface. Water droplets attached to the hydrophobic MEA surface and occupied a little part of the MEA surface. This was beneficial for gas transport into the gas diffusion layer and the water was easily swept out.

In Fig. 11(d), all the surfaces were hydrophobic. The water was congregated as a water column. In this case the MEA surface was hardly covered by water. But if there was large amount of water, the diameter and the length of the column would increase. This would lead to flow channel blockage.

4. Conclusions

(1) The material properties of the channel side-walls have a great influence on the water transport in a micro-channel. Not only the discharge intervals but also the water distribution in the channel changes with the material properties.
(2) The removal of water on a hydrophobic surface is faster than that on a hydrophilic surface.
(3) If a MEA surface is hydrophilic, a hydrophilic channel side-wall is beneficial to the gas transport into the gas diffusion layer.

(4) If the MEA surface is hydrophobic and the channel side-wall is hydrophilic, water can be dispersed into thin water films attached to the channel side-wall and water droplets are attached to the MEA surface. This is not only beneficial to water discharging but is also beneficial to gas transportation from the channel into the MEA.

Acknowledgements

The authors gratefully acknowledge the financial support from the National Natural Science Key Foundation of China (No. 50236010) and the State Key Development Program for basic Research of China (No. G2000026410).

References

[1] T.A. Zawodzinski, C. Derouin, S. Radzinsksi, R.J. Sherman, V.T. Smith, T.E. Springer, S. Gottesfeld, J. Electrochem. Soc. 140 (1993) 1041–1047.
[2] T.A. Zawodzinski, J. Davey, J.A. Valerio, S. Gottesfeld, Electrochim. Acta 40 (1995) 297–302.
[3] S. Motupally, A.J. Becker, J.W. Weidner, J. Electrochem. Soc. 147 (2000) 3171–3177.
[4] P. Choi, R. Datta, J. Electrochem. Soc. 150 (2003) E601–E607.
[5] U. Pasaogullari, C.Y. Wang, J. Electrochem. Soc. 151 (2004) A399–A406.
[6] A.Z. Weber, J. Newman, J. Electrochem. Soc. 152 (2005) A677–A688.
[7] T. Berning, N. Djilali, J. Electrochem. Soc. 150 (2003) A1598.
[8] S. Dutta, S. Shimpalee, J.W. Van Zee, Int. J. Heat Mass Transfer 44 (2001) 2029–2042.
[9] V. Gurau, H. Liu, S. Kakac, AIChE J. 44 (1998) 2410–2422.
[10] A. Golpaygan, N. Ashgriz, Int. J. Energy Res. 29 (2005) 1027–1040.
[11] P. Quan, B. Zhou, A. Sobiesiak, Z. Liu, J. Power Sources 152 (2005) 131–145.
[12] Z. Zhan, J. Xiao, M. Pan, R. Yuan, J. Power Sources 157 (2006) 226–243.
[13] K. Jiao, B. Zhou, P. Quan, J. Power Sources 154 (2006) 124–137.
[14] K. Jiao, B. Zhou, P. Quan, J. Power Sources, doi:10.1016/j.jpowsour.2005.06.041.
[15] R. Satija, D.L. Jacobson, M. Arif, S.A. Werner, J. Power Sources 129 (2004) 238–245.
[16] A.B. Geiger, A. Tsukada, E. Lehmann, Fuel Cells 2 (2003) 92–98.
[17] D. Kramer, J.B. Zhang, R. Shimoi, Electrochim. Acta 50 (2005) 2603–2614.
[18] K. Tüber, D. Pócza, C. Hebling, J. Power Sources 124 (2003) 403–414.
[19] X.G. Yang, F.Y. Zhang, A.L. Lubawy, C.Y. Wang, Electrochem. Solid-State Lett. 7 (2004) A408–A411.
[20] FLUENT 6.1.22 User's Guide, FLUENT, 2004.